21st Australasian Fluid Mechanics Conference
Adelaide, Australia
10-13 December 2018

Viscoelastic local dynamics of microtubes conveying fluid

Mergen H. Ghayesh[1], Ali Farajpour[1] and Hamed Farokhi[2]

[1]School of Mechanical Engineering
University of Adelaide, South Australia 5005, Australia

[2]Department of Mechanical and Construction Engineering,
Northumbria University, Newcastle upon Tyne NE1 8ST, UK

Abstract

In the present study, a nonlinear coupled scale-dependent continuum model is developed to examine the local dynamics of a pulsatile fluid-conveying microscale tube. The effect of the internal energy loss is described by the Kelvin-Voigt model of viscoelasticity. Parametric forces due to the pulsatile flow as well as Coriolis forces are taken into consideration in the nonlinear scale-dependent model. The Euler-Bernoulli beam theory is utilised for describing the deformation behaviour while scale effects are captured via the modified version of the theory of couple stress. Then, Hamilton's principle is utilised so as to derive the differential equations of the pulsatile fluid-conveying microscale tube. The local dynamic characteristics are determined near the parametric resonance of the viscoelastic microscale system in the supercritical regime.

Introduction

The influence of the internal energy friction, which plays a significant role in the dynamic behaviour of various fundamental structures such as elastic pipes, should be taken into consideration in order to develop an accurate continuum model for fluid-conveying macroscale structures. Furthermore, it has been recently shown that the internal energy friction can have a crucial effect on the oscillation response of structures at microscale levels [1].

As the net microfluid work on the microscale tube is negligible, the dynamic problem of fluid-conveying microscale tube is categorised in the class of conservative systems. For this type of microsystems, real values are always found for the natural frequencies inside the subcritical regime. By contrast, when a viscoelastic microtube contains a pulsatile flowing fluid, the microscale system is categorised as parametric gyroscopic non-conservative systems, in which the parametric resonance is usually observed near twice each natural frequency.

In recent years, some theoretical investigations have been done on the mechanics of ultrasmall structures containing fluid flow. First of all, it should be emphasised that at ultrasmall levels, size effects play an important role in the mechanical characteristics of structures [2-6]. Secondly, at microscales, the modified couple stress theory (MCST) [7, 8] is extensively employed for capturing size effects whereas the nonlocal theory [9, 10] is able to better incorporate these effects at nanoscales. Now the most relevant investigations are concisely reviewed. Xia and Wang [11] proposed a non-classical beam model to study the mechanical response of fluid-conveying micropipes. In another analysis, Kural and Özkaya [12] examined size effects on the vibrational response of microbeams containing fluid flow embedded in a linear elastic medium. A size-dependent strain gradient model was also developed in the literature for the instability of cantilever pipes at microscale levels [13]. Dai et al. [14] examined the pull-in mechanics of a fluid-conveying microscale beam actuated in an electrostatic way. Wang [15] also proposed a linear beam model for the fluid-induced vibrational response of microtubes with small deformations using the MCST. Furthermore, Abbasnejad et al. [16] investigated the instability of fluid-conveying microscale pipes actuated in a piezoelectric way; they did not take into account size effects. Yang et al. [17] applied the MCST to fluid-conveying microscale tubes in order to investigate their nonlinear vibration characteristics; a single-mode method was employed to determine an approximate solution. Dehrouyeh-Semnani et al. [18] also carried out a nonlinear stability analysis on geometrically imperfect microscale pipes containing fluid flow. A nonlocal strain gradient elasticity was also utilised in the literature to determine the critical fluid velocities of fluid-conveying ultrasmall pipes [19]. Moreover, the vibrational response of curved microscale tubes containing fluid flow was investigated by Tang et al. [20] with the help of the MCST. More lately, Hu et al. [21] has explored the linear mechanical characteristics of fluid-conveying microscale pipes with pined-free ends using the differential quadrature method as a numerical solution technique.

All of the studies reviewed above are restricted to microscale tubes containing fluid flow of a time-independent speed; in this study, an attempt is made to explore the large amplitude local dynamics of microtubes containing fluid flow of a time-dependent speed. The influences of the internal friction are incorporated in the nonlinear analysis. The Hamilton law of work/energy balance and the MCST are applied for deriving coupled motion equations. At the next stage, the decomposition of the motion equations is carried out employing Galerkin's procedure. At the final stage, a numerical integration technique is utilised to determine the local dynamic characteristics of the microsystem containing fluid flow. Numerical results for this ultrasmall system are presented near the first parametric resonance for exploring the viscoelastic local dynamics.

Size-dependent continuum modelling

Figure 1 shows a microtube conveying fluid flow of a time-dependent speed (i.e. $U(t)$. The microsystem is surrounded by a system of nonlinear springs; k_1 is the linear coefficient of the spring system, and k_2 represents the nonlinear coefficient. L, D and D_i are employed to indicate the length, outer and inner diameters of the microtube. Let us denote the axial strain, axial displacement, transverse deflection and rotation of the tube by ε_{xx}, u, v and ϕ, respectively. Using the Euler-Bernoulli theory, one can obtain

$$\varepsilon_{xx}(x,z,t)=\left[\left(1+\frac{\partial u(x,t)}{\partial x}\right)^2+\left(\frac{\partial v(x,t)}{\partial x}\right)^2\right]^{\frac{1}{2}} -1-z\frac{\partial \phi(x,t)}{\partial x}. \quad (1)$$

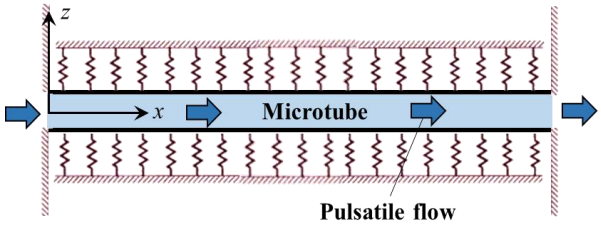

Figure 1. A microtube conveying fluid of a time-dependent speed.

According to the Kelvin-Voigt model, the total stress (σ_{xx}), the elastic stress $(\sigma_{xx(el)})$ and the viscoelastic stress $(\sigma_{xx(vis)})$ are expressed as

$$\sigma_{xx}=\sigma_{xx(el)}+\sigma_{xx(vis)},\quad \begin{Bmatrix}\sigma_{xx(el)}\\ \sigma_{xx(vis)}\end{Bmatrix}=\begin{Bmatrix}E\varepsilon_{xx}\\ c_{vis}\dfrac{\partial\varepsilon_{xx}}{\partial t}\end{Bmatrix}, \tag{2}$$

in which E and c_{vis} indicate the elasticity and viscosity constants of the microtube, respectively. Applying the MCST, symmetric rotation-gradient components (χ_{ij}) can be written as

$$\begin{Bmatrix}\chi_{xy}\\ \chi_{yz}\end{Bmatrix}=-\frac{1}{4}\frac{\partial}{\partial x}\begin{Bmatrix}\sin\phi+\dfrac{\partial v}{\partial x}\\ \cos\phi\end{Bmatrix}-\frac{z}{4}\frac{\partial^2}{\partial x^2}\begin{Bmatrix}\cos\phi\\ 0\end{Bmatrix}. \tag{3}$$

In addition, the symmetric deviatoric couple-stress components (m_{ij}) are as follows

$$\begin{Bmatrix}m_{xy}\\ m_{yz}\end{Bmatrix}=\begin{Bmatrix}m_{xy(el)}+m_{xy(vis)}\\ m_{yz(el)}+m_{yz(vis)}\end{Bmatrix},$$

$$\begin{Bmatrix}m_{xy(el)}\\ m_{yz(el)}\end{Bmatrix}=\frac{l^2E}{1+\nu}\begin{Bmatrix}\chi_{xy}\\ \chi_{yz}\end{Bmatrix},\quad \begin{Bmatrix}m_{xy(vis)}\\ m_{yz(vis)}\end{Bmatrix}=\frac{l^2c_{vis}}{1+\nu}\frac{\partial}{\partial t}\begin{Bmatrix}\chi_{xy}\\ \chi_{yz}\end{Bmatrix}, \tag{4}$$

where ν and l denote the Poisson's ratio and the length-scale parameter, respectively. The speed of the microscale fluid flow (i.e. u_f) is assumed as

$$u_f=u_{f0}+u_{f1}\cos\left(\Omega_f\bar{t}\right), \tag{5}$$

where u_{f0}, u_{f1} $\bar{t}$, and Ω_f are respectively the dimensionless mean fluid speed, speed amplitude, time and pulsatile flow frequency, which are, respectively, defined by $u_{f0}=U_0\sqrt{L^2M/EI}$, $u_{f1}=U_1\sqrt{L^2M/EI}$, $\bar{t}=t\sqrt{EI/L^4(M+m)}$ and $\Omega_f=\omega\sqrt{L^4(M+m)/EI}$. The plug flow is assumed since the thickness of the boundary layer is very small. Let us denote the kinetic energy, the elastic energy, the work due to the viscoelasticity and the elastic energy of the spring bed by T_k, U_{el}, W_{vis} and U_s, respectively. Moreover, M, m, A and I are utilised to denote the fluid mass per length, the tube mass per length, the area and inertia moment of the tube cross-section, respectively. The microscale beam is made of epoxy polymeric materials with the materials properties given in next section. The microtube is assumed to be subject to axial pretention (i.e. T_0). The Hamilton principle is given by

$$\int_{t_1}^{t_2}\left(\delta T_k+\delta W_{vis}-\delta U_s-\delta U_{el}\right)\mathrm{d}t=0. \tag{6}$$

For convenience, the following non-dimensional parameters are implemented

$$\begin{aligned}&\bar{x}=\frac{x}{L},\quad \begin{Bmatrix}\bar{u}\\ \bar{v}\end{Bmatrix}=\frac{1}{D}\begin{Bmatrix}u\\ v\end{Bmatrix},\quad \beta=\frac{M/m}{M/m+1},\quad \Xi_g=\frac{L^2A}{I},\\ &\Gamma=\frac{L^2T_0}{EI},\quad \gamma=\frac{L}{D},\ K_1=\frac{L^4}{EI}k_1,\quad K_2=\frac{L^4D^2}{EI}k_2,\\ &\alpha_{vis}=\sqrt{\frac{EI}{(M+m)L^4}}\frac{c_{vis}}{E},\quad \bar{\mu}=\frac{l^2A}{2I(1+\nu)}.\end{aligned} \tag{7}$$

Using the above equations, the non-dimensional nonlinear coupled equations of motion are derived as

$$\begin{aligned}&\frac{\partial^2\bar{u}}{\partial\bar{t}^2}-\gamma\Omega_fu_{f1}\sqrt{\beta}\sin\left(\Omega_f\bar{t}\right)-\Omega_fu_{f1}\sqrt{\beta}\sin\left(\Omega_f\bar{t}\right)\frac{\partial\bar{u}}{\partial\bar{x}}\\ &+\left[u_{f0}+u_{f1}\cos\left(\Omega_f\bar{t}\right)\right]^2\frac{\partial^2\bar{u}}{\partial\bar{x}^2}-\Xi_g\frac{\partial^2\bar{u}}{\partial\bar{x}^2}+2u_{f0}\sqrt{\beta}\frac{\partial^2\bar{u}}{\partial\bar{x}\partial\bar{t}}\\ &+2u_{f1}\sqrt{\beta}\cos\left(\Omega_f\bar{t}\right)\frac{\partial^2\bar{u}}{\partial\bar{x}\partial\bar{t}}-\frac{\Xi_g}{\gamma}\frac{\partial^2\bar{v}}{\partial\bar{x}^2}\frac{\partial\bar{v}}{\partial\bar{x}}\\ &-\left(\frac{1}{\gamma}+\frac{\bar{\mu}}{2\gamma}\right)\left(\frac{\partial^3\bar{v}}{\partial\bar{x}^3}\frac{\partial^2\bar{v}}{\partial\bar{x}^2}+\frac{\partial^4\bar{v}}{\partial\bar{x}^4}\frac{\partial\bar{v}}{\partial\bar{x}}\right)\\ &-\frac{1}{\gamma}\alpha_{vis}\Xi_g\left(\gamma\frac{\partial^3\bar{u}}{\partial\bar{t}\partial\bar{x}^2}+\frac{\partial^2\bar{v}}{\partial\bar{t}\partial\bar{x}}\frac{\partial^2\bar{v}}{\partial\bar{x}^2}+\frac{\partial^3\bar{v}}{\partial\bar{t}\partial\bar{x}^2}\frac{\partial\bar{v}}{\partial\bar{x}}\right)\\ &-\left(\frac{\alpha_{vis}}{\gamma}+\frac{\bar{\mu}\alpha_{vis}}{2\gamma}\right)\left(\frac{\partial^4\bar{v}}{\partial\bar{t}\partial\bar{x}^3}\frac{\partial^2\bar{v}}{\partial\bar{x}^2}+\frac{\partial^5\bar{v}}{\partial\bar{t}\partial\bar{x}^4}\frac{\partial\bar{v}}{\partial\bar{x}}\right)=0,\end{aligned} \tag{8}$$

$$\begin{aligned}&\frac{\partial^2\bar{v}}{\partial\bar{t}^2}-u_{f1}\Omega_f\sqrt{\beta}\sin\left(\Omega_f\bar{t}\right)\frac{\partial\bar{v}}{\partial\bar{x}}-\Gamma\frac{\partial^2\bar{v}}{\partial\bar{x}^2}+K_2\bar{v}^3\\ &+K_1\bar{v}+\left(1+\bar{\mu}\right)\frac{\partial^4\bar{v}}{\partial\bar{x}^4}+\left[u_{f0}+u_{f1}\cos\left(\Omega_f\bar{t}\right)\right]^2\frac{\partial^2\bar{v}}{\partial\bar{x}^2}\\ &+2u_{f0}\sqrt{\beta}\frac{\partial^2\bar{v}}{\partial\bar{t}\partial\bar{x}}+2u_{f1}\sqrt{\beta}\cos\left(\Omega_f\bar{t}\right)\frac{\partial^2\bar{v}}{\partial\bar{t}\partial\bar{x}}\\ &-\frac{3\Xi_g}{2\gamma^2}\frac{\partial^2\bar{v}}{\partial\bar{x}^2}\left(\frac{\partial\bar{v}}{\partial\bar{x}}\right)^2-\frac{\Xi_g}{\gamma}\left(\frac{\partial\bar{v}}{\partial\bar{x}}\frac{\partial^2\bar{u}}{\partial\bar{x}^2}+\frac{\partial^2\bar{v}}{\partial\bar{x}^2}\frac{\partial\bar{u}}{\partial\bar{x}}\right)\\ &-\frac{1}{\gamma}\left\{3\frac{\partial^2\bar{v}}{\partial\bar{x}^2}\frac{\partial^3\bar{u}}{\partial\bar{x}^3}+2\frac{\partial^4\bar{v}}{\partial\bar{x}^4}\frac{\partial\bar{u}}{\partial\bar{x}}+4\frac{\partial^3\bar{v}}{\partial\bar{x}^3}\frac{\partial^2\bar{u}}{\partial\bar{x}^2}+\frac{\partial\bar{v}}{\partial\bar{x}}\frac{\partial^4\bar{u}}{\partial\bar{x}^4}\right.\\ &\left.+\frac{1}{\gamma}\left[2\left(\frac{\partial^2\bar{v}}{\partial\bar{x}^2}\right)^3+8\frac{\partial\bar{v}}{\partial\bar{x}}\frac{\partial^3\bar{v}}{\partial\bar{x}^3}\frac{\partial^2\bar{v}}{\partial\bar{x}^2}+2\frac{\partial^4\bar{v}}{\partial\bar{x}^4}\left(\frac{\partial\bar{v}}{\partial\bar{x}}\right)^2\right]\right\}\\ &-\frac{\bar{\mu}}{4\gamma}\left\{6\frac{\partial^2\bar{v}}{\partial\bar{x}^2}\frac{\partial^3\bar{u}}{\partial\bar{x}^3}+4\frac{\partial^4\bar{v}}{\partial\bar{x}^4}\frac{\partial\bar{u}}{\partial\bar{x}}+8\frac{\partial^3\bar{v}}{\partial\bar{x}^3}\frac{\partial^2\bar{u}}{\partial\bar{x}^2}+2\frac{\partial\bar{v}}{\partial\bar{x}}\frac{\partial^4\bar{u}}{\partial\bar{x}^4}\right.\\ &\left.+\frac{1}{\gamma}\left[20\frac{\partial^2\bar{v}}{\partial\bar{x}^2}\frac{\partial\bar{v}}{\partial\bar{x}}\frac{\partial^3\bar{v}}{\partial\bar{x}^3}+5\frac{\partial^4\bar{v}}{\partial\bar{x}^4}\left(\frac{\partial\bar{v}}{\partial\bar{x}}\right)^2+5\left(\frac{\partial^2\bar{v}}{\partial\bar{x}^2}\right)^3\right]\right\}\\ &-\frac{\bar{\mu}}{4\gamma^2\Xi_g}\left[3\left(\frac{\partial^3\bar{v}}{\partial\bar{x}^3}\right)^2\frac{\partial^2\bar{v}}{\partial\bar{x}^2}+6\frac{\partial\bar{v}}{\partial\bar{x}}\frac{\partial^5\bar{v}}{\partial\bar{x}^5}\frac{\partial^2\bar{v}}{\partial\bar{x}^2}+10\frac{\partial\bar{v}}{\partial\bar{x}}\frac{\partial^4\bar{v}}{\partial\bar{x}^4}\frac{\partial^3\bar{v}}{\partial\bar{x}^3}\right.\\ &\left.+4\frac{\partial^4\bar{v}}{\partial\bar{x}^4}\left(\frac{\partial^2\bar{v}}{\partial\bar{x}^2}\right)^2+\frac{\partial^6\bar{v}}{\partial\bar{x}^6}\left(\frac{\partial\bar{v}}{\partial\bar{x}}\right)^2\right]-\frac{\alpha_{vis}\Xi_g}{\gamma^2}\left[\frac{\partial^3\bar{v}}{\partial\bar{t}\partial\bar{x}^2}\left(\frac{\partial\bar{v}}{\partial\bar{x}}\right)^2\right.\\ &\left.+2\frac{\partial\bar{v}}{\partial\bar{x}}\frac{\partial^2\bar{v}}{\partial\bar{t}\partial\bar{x}}\frac{\partial^2\bar{v}}{\partial\bar{x}^2}\right]-\frac{\alpha_{vis}\Xi_g}{\gamma}\left(\frac{\partial\bar{v}}{\partial\bar{x}}\frac{\partial^3\bar{u}}{\partial\bar{t}\partial\bar{x}^2}+\frac{\partial^2\bar{v}}{\partial\bar{x}^2}\frac{\partial^2\bar{u}}{\partial\bar{t}\partial\bar{x}}\right)\\ &+\alpha_{vis}\frac{\partial^5\bar{v}}{\partial\bar{t}\partial\bar{x}^4}-\frac{\alpha_{vis}}{\gamma}\left(\frac{\partial^5\bar{u}}{\partial\bar{t}\partial\bar{x}^4}\frac{\partial\bar{v}}{\partial\bar{x}}+\frac{\partial^4\bar{u}}{\partial\bar{x}^4}\frac{\partial^2\bar{v}}{\partial\bar{t}\partial\bar{x}}+\frac{\partial^2\bar{u}}{\partial\bar{t}\partial\bar{x}}\frac{\partial^4\bar{v}}{\partial\bar{x}^4}\right.\\ &\left.+3\frac{\partial^3\bar{u}}{\partial\bar{t}\partial\bar{x}^2}\frac{\partial^3\bar{v}}{\partial\bar{x}^3}+2\frac{\partial^5\bar{v}}{\partial\bar{t}\partial\bar{x}^4}\frac{\partial\bar{u}}{\partial\bar{x}}+3\frac{\partial^2\bar{v}}{\partial\bar{x}^2}\frac{\partial^4\bar{u}}{\partial\bar{t}\partial\bar{x}^3}\right.\\ &\left.+4\frac{\partial^4\bar{v}}{\partial\bar{t}\partial\bar{x}^3}\frac{\partial^2\bar{u}}{\partial\bar{x}^2}+3\frac{\partial^3\bar{v}}{\partial\bar{t}\partial\bar{x}^2}\frac{\partial^3\bar{u}}{\partial\bar{x}^3}\right)-\frac{\alpha_{vis}}{\gamma^2}\left[6\frac{\partial^2\bar{v}}{\partial\bar{x}^2}\frac{\partial^2\bar{v}}{\partial\bar{t}\partial\bar{x}}\frac{\partial^3\bar{v}}{\partial\bar{x}^3}\right.\\ &\left.+8\frac{\partial\bar{v}}{\partial\bar{x}}\frac{\partial^4\bar{v}}{\partial\bar{t}\partial\bar{x}^3}\frac{\partial^2\bar{v}}{\partial\bar{x}^2}+6\frac{\partial\bar{v}}{\partial\bar{x}}\frac{\partial^3\bar{v}}{\partial\bar{x}^3}\frac{\partial^3\bar{v}}{\partial\bar{t}\partial\bar{x}^2}+2\frac{\partial^5\bar{v}}{\partial\bar{t}\partial\bar{x}^4}\left(\frac{\partial\bar{v}}{\partial\bar{x}}\right)^2\right.\\ &\left.+6\frac{\partial^3\bar{v}}{\partial\bar{t}\partial\bar{x}^2}\left(\frac{\partial^2\bar{v}}{\partial\bar{x}^2}\right)^2+2\frac{\partial\bar{v}}{\partial\bar{x}}\frac{\partial^2\bar{v}}{\partial\bar{t}\partial\bar{x}}\frac{\partial^4\bar{v}}{\partial\bar{x}^4}\right]\end{aligned}$$

$$+\alpha_{vis}\bar{\mu}\frac{\partial^5\bar{v}}{\partial\bar{t}\,\partial\bar{x}^4}-\frac{\alpha_{vis}\bar{\mu}}{4\gamma}\left(2\frac{\partial\bar{v}}{\partial\bar{x}}\frac{\partial^5\bar{u}}{\partial\bar{t}\,\partial\bar{x}^4}+2\frac{\partial^2\bar{v}}{\partial\bar{t}\,\partial\bar{x}}\frac{\partial^4\bar{u}}{\partial\bar{x}^4}\right.$$
$$+6\frac{\partial^3\bar{v}}{\partial\bar{x}^3}\frac{\partial^3\bar{u}}{\partial\bar{t}\,\partial\bar{x}^2}+6\frac{\partial^2\bar{v}}{\partial\bar{x}^2}\frac{\partial^4\bar{u}}{\partial\bar{t}\,\partial\bar{x}^3}+6\frac{\partial^3\bar{v}}{\partial\bar{t}\,\partial\bar{x}^2}\frac{\partial^3\bar{u}}{\partial\bar{x}^3}$$
$$\left.+2\frac{\partial^4\bar{v}}{\partial\bar{x}^4}\frac{\partial^2\bar{u}}{\partial\bar{t}\,\partial\bar{x}}+8\frac{\partial^4\bar{v}}{\partial\bar{t}\,\partial\bar{x}^3}\frac{\partial^2\bar{u}}{\partial\bar{x}^2}+4\frac{\partial^5\bar{v}}{\partial\bar{t}\,\partial\bar{x}^4}\frac{\partial\bar{u}}{\partial\bar{x}}\right)$$
$$-\frac{\alpha_{vis}\bar{\mu}}{4\gamma^2}\left(15\frac{\partial^3\bar{v}}{\partial\bar{t}\,\partial\bar{x}^2}\frac{\partial\bar{v}}{\partial\bar{x}}\frac{\partial^3\bar{v}}{\partial\bar{x}^3}+17\frac{\partial^2\bar{v}}{\partial\bar{x}^2}\frac{\partial^2\bar{v}}{\partial\bar{t}\,\partial\bar{x}}\frac{\partial^3\bar{v}}{\partial\bar{x}^3}\right.$$
$$+16\frac{\partial^3\bar{v}}{\partial\bar{t}\,\partial\bar{x}^2}\left(\frac{\partial^2\bar{v}}{\partial\bar{x}^2}\right)^2+20\frac{\partial\bar{v}}{\partial\bar{x}}\frac{\partial^4\bar{v}}{\partial\bar{t}\,\partial\bar{x}^3}\frac{\partial^2\bar{v}}{\partial\bar{x}^2}+$$
$$5\frac{\partial\bar{v}}{\partial\bar{x}}\frac{\partial^4\bar{v}}{\partial\bar{x}^4}\frac{\partial^2\bar{v}}{\partial\bar{t}\,\partial\bar{x}}+5\frac{\partial^5\bar{v}}{\partial\bar{t}\,\partial\bar{x}^4}\left(\frac{\partial\bar{v}}{\partial\bar{x}}\right)^2\Bigg)-\frac{\bar{\mu}\alpha_{vis}}{4\Xi_g\gamma^2}\left[\frac{\partial^7\bar{v}}{\partial\bar{t}\,\partial\bar{x}^6}\left(\frac{\partial\bar{v}}{\partial\bar{x}}\right)^2\right.$$
$$+5\frac{\partial^3\bar{v}}{\partial\bar{t}\,\partial\bar{x}^2}\frac{\partial\bar{v}}{\partial\bar{x}}\frac{\partial^5\bar{v}}{\partial\bar{x}^5}+\frac{\partial^2\bar{v}}{\partial\bar{x}^2}\frac{\partial^2\bar{v}}{\partial\bar{t}\,\partial\bar{x}}\frac{\partial^5\bar{v}}{\partial\bar{x}^5}+6\frac{\partial^2\bar{v}}{\partial\bar{x}^2}\frac{\partial\bar{v}}{\partial\bar{x}}\frac{\partial^6\bar{v}}{\partial\bar{t}\,\partial\bar{x}^5}$$
$$+4\frac{\partial^3\bar{v}}{\partial\bar{t}\,\partial\bar{x}^2}\frac{\partial^2\bar{v}}{\partial\bar{x}^2}\frac{\partial^4\bar{v}}{\partial\bar{x}^4}+\frac{\partial^6\bar{v}}{\partial\bar{x}^6}\frac{\partial\bar{v}}{\partial\bar{x}}\frac{\partial^2\bar{v}}{\partial\bar{t}\,\partial\bar{x}}$$
$$+6\frac{\partial^4\bar{v}}{\partial\bar{t}\,\partial\bar{x}^3}\frac{\partial^3\bar{v}}{\partial\bar{x}^3}\frac{\partial^2\bar{v}}{\partial\bar{x}^2}+10\frac{\partial\bar{v}}{\partial\bar{x}}\frac{\partial^4\bar{v}}{\partial\bar{x}^4}\frac{\partial^4\bar{v}}{\partial\bar{t}\,\partial\bar{x}^3}$$
$$\left.\left.+4\frac{\partial^5\bar{v}}{\partial\bar{t}\,\partial\bar{x}^4}\left(\frac{\partial^2\bar{v}}{\partial\bar{x}^2}\right)^2+10\frac{\partial^5\bar{v}}{\partial\bar{t}\,\partial\bar{x}^4}\frac{\partial\bar{v}}{\partial\bar{x}}\frac{\partial^3\bar{v}}{\partial\bar{x}^3}\right]=0.\right. \tag{9}$$

For discretisation, the displacement components of the microscale tube can be written as

$$\bar{u}=\sum_{m=1}^{N_u}\tilde{u}_m(\bar{x})r_m\,,\quad \bar{v}=\sum_{m=1}^{N_v}\tilde{v}_m(\bar{x})q_m\,, \tag{10}$$

In Eq. (10), $\tilde{u}_m$, r_m, $\tilde{v}_m$ and q_m are respectively the axial shape function, the axial generalised coordinate, the transverse shape function and the transverse generalised coordinate. Applying Galerkin's method and a continuation scheme, a solution is found for clamped-clamped ends. Equations (8) and (9) are solved concurrently and it leads to a unique solution but the amplitudes of the transverse and axial motions can be different.

Numerical results

The mechanical properties of the viscoelastic microtube are set to E=1.44 GPa, ν=0.38, α_{vis}=0.0003, γ=120, $\bar{\mu}$=0.3883, ρ_p=1220 kg/m^3 and ρ_f =1000 kg/m^3 in which ρ_p and ρ_f indicate the density of the tube and fluid, respectively [22]. The microsystem geometrical properties are also taken as D_i=40 μm, D=55 μm, L/D = 120, Ξ_g =1.5069×10^5 and β=0.4793. The dimensionless pretention is set to Γ =5.0 while the dimensionless spring stiffnesses are K_1=50.0 and K_2=0.0.

Figure 2 illustrates the parametric resonance behaviour of microscale tubes containing pulsatile flowing fluid for the transverse motion. It is assumed that the viscoelastic microsystem is in the supercritical regime. It should be noticed that the model can predict the onset of the instability. However, to avoid giving many results and figures, only the results of the supercritical regime are considered. The mean speed and amplitude of the pulsatile fluid are taken as u_{f0}=10 and u_{f1}=0.10, respectively. The viscoelastic microtube conveying pulsatile flow displays a softening-type nonlinearity. Furthermore, two period doubling (PD) points are observed for the viscoelastic microsystem. One saddle (SD) point is also found in the local dynamic response of microtubes conveying pulsatile fluid.

The parametric resonance behaviour of microscale tubes containing pulsatile flowing fluid for the axial motion is shown in Fig. 3. The viscoelastic microtube is assumed to be in the supercritical regime. The fluid pulsation is characterised by u_{f0}=10 and u_{f1}=0.10. The axial motion is also of a softening-type nonlinearity in the supercritical regime. In addition, two distinct period doubling points as well as one saddle point are found for the axial motion.

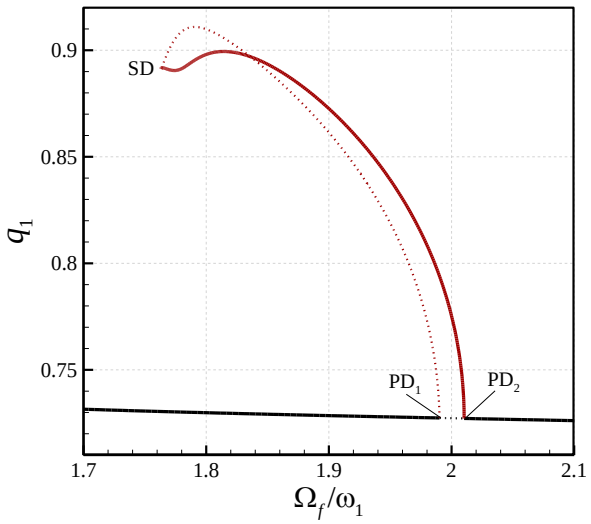

Figure 2. Parametric resonance of microscale tubes containing pulsatile fluid for the transverse motion.

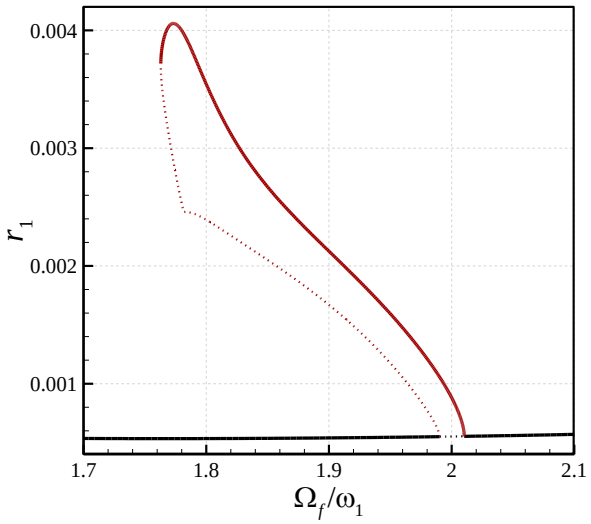

Figure 3. Parametric resonance of microscale tubes containing pulsatile fluid for the axial motion.

In Fig. 4, the parametric resonance behaviour of microscale tubes containing pulsatile flowing fluid is plotted for different mean values of the fluid speed. The results are presented for the first generalised coordinate of the transverse motion. The mean value of the pulsatile flowing fluid varies from u_{f0}=9.75 to u_{f0}=10.25 while the amplitude of the pulsatile flow is set to u_{f1}=0.10. The region of the parametric resonance shifts to the right side by a slight increase in the mean value of the pulsatile flowing fluid. Moreover, the transverse amplitude significantly increases by a slight increase in the mean fluid speed.

Figure 5 depicts the parametric resonance of microscale tubes containing pulsatile fluid for the axial motion for different mean values of the fluid speed. It is found that higher mean speeds result in higher parametric resonance frequencies. In addition, the amplitude of the transverse motion remarkably increases by a small increase in the mean speed in the supercritical regime.

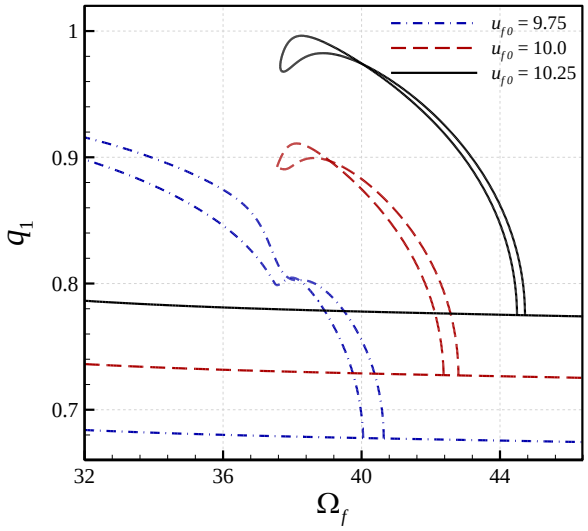

Figure 4. Parametric resonance of microscale tubes containing fluid for different mean fluid speeds for the transverse motion.

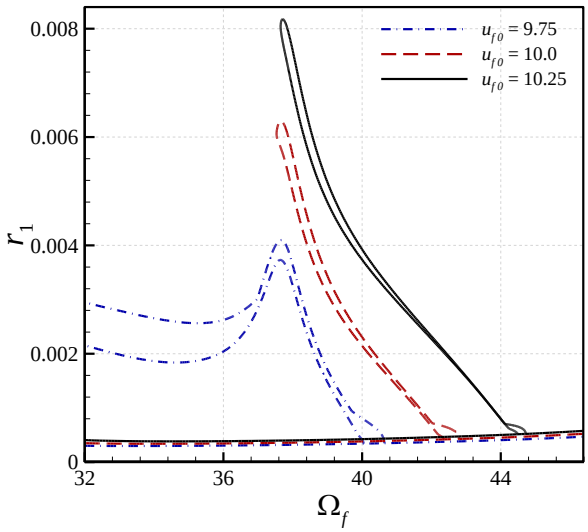

Figure 5. Parametric resonance of microscale tubes containing fluid for different mean fluid speeds for the axial motion.

Conclusions

A nonlinear scale-dependent continuum model was developed to study the local dynamics of pulsatile fluid-conveying microtubes. Parametric forces caused by the pulsatile flow and Coriolis forces were incorporated. Scale effects were captured employing the MCST. Hamilton's principle was utilised for deriving the differential equations of the microscale system. The local dynamic characteristics were obtained near the parametric resonance of the system in the supercritical regime. The microscale tube conveying pulsatile flow exhibits a softening-type nonlinearity with two PD points and one SD point. Furthermore, higher values for the mean speed of the pulsatile fluid lead to higher parametric resonance frequencies.

References

[1] Doaré O. Dissipation effect on local and global stability of fluid-conveying pipes. J. Sound Vib. 2010;329:72-83.

[2] Reddy J. Nonlocal theories for bending, buckling and vibration of beams. Int. J. Eng. Sci. 2007;45:288-307.

[3] Sudak L. Column buckling of multiwalled carbon nanotubes using nonlocal continuum mechanics. J. Appl. Phys. 2003;94:7281-7.

[4] Park S, Gao X. Bernoulli–Euler beam model based on a modified couple stress theory. J. Micromech. Microeng. 2006;16:2355.

[5] Farajpour M, Shahidi A, Tabataba'i-Nasab F, Farajpour A. Vibration of initially stressed carbon nanotubes under magneto-thermal environment for nanoparticle delivery via higher-order nonlocal strain gradient theory. EPJ Plus. 2018;133:219.

[6] Farajpour MR, Rastgoo A, Farajpour A, Mohammadi M. Vibration of piezoelectric nanofilm-based electromechanical sensors via higher-order non-local strain gradient theory. Micro & Nano Lett. 2016;11:302-7.

[7] Ma H, Gao X-L, Reddy J. A microstructure-dependent Timoshenko beam model based on a modified couple stress theory. J. Mech. Phys. Solids. 2008;56:3379-91.

[8] Ghayesh MH, Farokhi H, Gholipour A, Tavallaeinejad M. Nonlinear oscillations of functionally graded microplates. Int. J. Eng. Sci. 2018;122:56-72.

[9] Aydogdu M. A nonlocal rod model for axial vibration of double-walled carbon nanotubes including axial van der Waals force effects. J. Vib. Control. 2015;21:3132-54.

[10] Farajpour M, Shahidi A, Farajpour A. A nonlocal continuum model for the biaxial buckling analysis of composite nanoplates with shape memory alloy nanowires. Mater. Res. Express. 2018;5:035026.

[11] Xia W, Wang L. Microfluid-induced vibration and stability of structures modeled as microscale pipes conveying fluid based on non-classical Timoshenko beam theory. Microfluid Nanofluidics. 2010;9:955-62.

[12] Kural S, Özkaya E. Size-dependent vibrations of a micro beam conveying fluid and resting on an elastic foundation. J. Vib. Control. 2017;23:1106-14.

[13] Hosseini M, Bahaadini R. Size dependent stability analysis of cantilever micro-pipes conveying fluid based on modified strain gradient theory. Int. J. Eng. Sci. 2016;101:1-13.

[14] Dai H, Wang L, Ni Q. Dynamics and pull-in instability of electrostatically actuated microbeams conveying fluid. Microfluid Nanofluidics. 2015;18:49-55.

[15] Wang L. Size-dependent vibration characteristics of fluid-conveying microtubes. J. Fluid Struct. 2010;26:675-84.

[16] Abbasnejad B, Shabani R, Rezazadeh G. Stability analysis of a piezoelectrically actuated micro-pipe conveying fluid. Microfluid nanofluidics. 2015;19:577-84.

[17] Yang T-Z, Ji S, Yang X-D, Fang B. Microfluid-induced nonlinear free vibration of microtubes. International Journal of Engineering Science. 2014;76:47-55.

[18] Dehrouyeh-Semnani AM, Nikkhah-Bahrami M, Yazdi MRH. On nonlinear stability of fluid-conveying imperfect micropipes. Int. J. Eng. Sci. 2017;120:254-71.

[19] Li L, Hu Y, Li X, Ling L. Size-dependent effects on critical flow velocity of fluid-conveying microtubes via nonlocal strain gradient theory. Microfluid nanofluidics. 2016;20:76.

[20] Tang M, Ni Q, Wang L, Luo Y, Wang Y. Nonlinear modeling and size-dependent vibration analysis of curved microtubes conveying fluid based on modified couple stress theory. Int. J. Eng. Sci. 2014;84:1-10.

[21] Hu K, Dai H, Wang L, Qian Q. Dynamics and Stability of Pinned-Free Micropipes Conveying Fluid. J. Mech. 2017:1-7.

[22] Lam DC, Yang F, Chong A, Wang J, Tong P. Experiments and theory in strain gradient elasticity, J. Mech. Phys. Solids 2003;51:1477-1508.